IIETA International Information and Engineering Technology Association
Advancing the World of Information and Engineering

Instrumentation Mesure Métrologie
vol. 24, no. 5, October, 2025, pp. 317-324
Journal homepage: http://iieta.org/journals/i2m

Experimental Hydraulic Investigation of Various Geometric Labyrinth Side Weirs

Safa Ibrahim Hasan*, Asmaa Abdul Jabbar Jamel

Dams and Water Resources Engineering Department, College of Engineering, Tikrit University, Tikrit 34001, Iraq

Corresponding Author Email: safaa.i.hassan@tu.edu.iq

https://doi.org/10.18280/i2m.240503

Received: 19 September 2025
Revised: 20 October 2025
Accepted: 25 October 2025
Available online: 31 October 2025

Keywords:
discharge coefficient, lateral weir, open channel, subcritical flow, hydraulic characteristics, water surface profile, trapezoidal labyrinth, arced labyrinth

ABSTRACT

Efficient management of excess water in confined channels is a critical challenge, especially under potential flood conditions caused by climate change. This paper presents an experimental investigation comparing the hydraulic characteristics of several labyrinth side weirs. Physical models were constructed using dimensional analysis to determine the parameters that affect the discharge coefficient (C_d) across different geometries. Using these models, tests were conducted on four labyrinth side weir configurations: trapezoidal ($\theta = 0°$) and arced-trapezoidal ($\theta = 20°$), each with sidewall angles $\alpha = 6°$ and $12°$ (5 cycles). The study aims to develop analytical equations to estimate the discharge coefficient of various labyrinth-side weirs under subcritical flow conditions. The results indicate that the arced-trapezoidal model with a 6° sidewall angle shows the highest discharge efficiency. A lower sidewall angle enhances the flow rate by effectively increasing the crest length. Four empirical equations were derived by nonlinear regression analysis. Their accuracy was confirmed using root mean square error (RMSE), average percentage error (APE), and coefficient of determination (R^2). The obtained values of 5%, 2%, and 0.99%, respectively, indicate strong agreement with the experimental results of this study.

1. INTRODUCTION

Side weirs are hydraulic structures widely used to divert excess water from a main channel into secondary channels, maintaining the design capacity of the main channel and supporting applications such as irrigation, drainage, wastewater management, and flood control [1-3]. Linear rectangular side weirs often require long openings along the main channel, which can complicate water depth regulation and reduce overall efficiency.

In contrast, labyrinth side weirs increase the effective crest length while limiting the required channel opening, enhancing flow capacity while minimizing the energy of flowing water, making them both effective and economical solutions [4-6]. The total length of a labyrinth weir is typically three to five times its width, and its discharge capacity depends on the upstream head, often reaching about twice that of a standard weir or overflow crest of the same width [4, 7]. Early studies established the fundamental principles of labyrinth weir design [5], demonstrating that labyrinth side weirs can achieve discharge capacities 1.5–4.5 times greater than conventional linear weirs of the same channel length [6]. However, increasing the number of cycles can increase negative effects such as nappe interference and flow collisions [8, 9]. Among labyrinth weirs, trapezoidal and arced-trapezoidal configurations are particularly valuable due to their practical advantages in open-channel flow management. Experimental and numerical studies have shown that these geometries achieve higher discharge coefficients (C_d) than traditional designs, with performance strongly influenced by key geometric parameters such as cycle number, sidewall angle, crest shape and length, and weir height relative to the upstream depth [4, 6-7, 10-16]. Field applications, including the Isabella Dam project, have validated these designs, confirming their capacity to safely manage Probable Maximum Floods using both physical and CFD modeling [17, 18]. Complementary theoretical studies have further established reliable methods for estimating C_d under subcritical flow, demonstrating the effect of upstream Froude number (Fr_1) and dimensionless parameters (p/y_1, B/y_1) on hydraulic performance [19-23].

Despite these advances, limited studies have focused specifically on trapezoidal and arced-trapezoidal labyrinth side weirs in a reservoir application under controlled laboratory conditions, particularly exploring a wide range of geometric parameters. Building on previous studies of design models [8], this study aims to enhance the applicability of labyrinth side-weir geometries in open-channel systems. The objective is to analytically investigate the effect of dimensionless parameters, in particular, upstream Froude number (Fr_1) and dimensionless parameters (p/y_1), (B/y_1), α, and θ, on discharge coefficient and to develop practical discharge coefficient equations for engineering use, thereby extending previous findings.

2. COEFFICIENT DISCHARGE FOR LABYRINTH SIDE WEIR

Marchi [24] was the first to propose a mathematical relationship for side-weir flow Eq. (1). This contribution significantly influenced experimental and theoretical studies in weir hydraulics, forming the foundation for further research in the field.

$$Q_s = \frac{2}{3} C_d \sqrt{2g} L (y_1 - p)^{3/2} \quad (1)$$

where, (Q_s) is the overall side weir discharge, (C_d) is the discharge coefficient (De Marchi coefficient), (g) is gravity's acceleration, (L) is side weir width, (y_1) is upstream flow depth at the channel centerline, and (p) is crest height are also considered as shown in Figure 1 [25, 26].

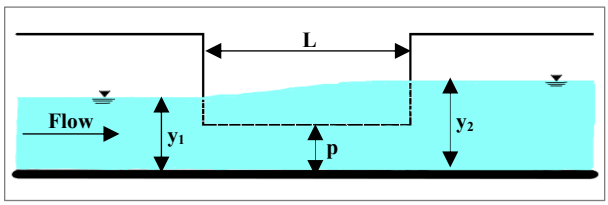

Figure 1. The longitudinal flow profile of subcritical flow at the side weir

3. DIMENSIONAL ANALYSIS OF LABYRINTH SIDE WEIR

One of the primary techniques for analyzing and relating to physical quantities in science and engineering is dimensional analysis. It depends on expressing amounts in terms of basic units such as mass (M), length (L), and time (T), and finding relationships between them [27].

Dimensional analysis is used to simplify the complexity of flow over hydraulic structures. It uses Buckingham's Pi (π-Theorem), a known mathematical method for formulating and interpreting relationships in physical and experimental studies. The consistency of the relationship between the discharge coefficient and the dimensionless independent variables is necessary for developing reliable models and informing more effective experimental design (see Figure 2). Table 1 shows the parameters for a labyrinth side weir as a function of several hydraulic and fluid properties.

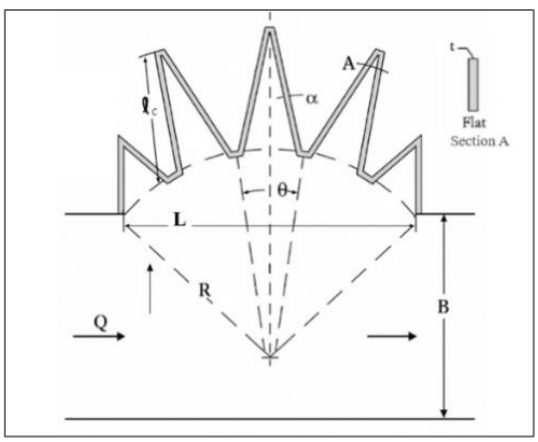

Figure 2. The side weir model geometric parameters design

Table 1. Parameters and dimensions in MLT's dimensional analysis system

Symbol	Description	Dimension
B	Channel width	L
g	Gravity acceleration	LT^{-2}
L	Side weir width	L
ℓ	Crest length	L
p	Side weir height	L
V_1	Upstream average velocity across the channel cross-section	LT^{-1}
y_1	Upstream flow depth at the channel centreline	L
α	Sidewall angle	-
θ	Arc angle for the cycle	-
μ	Water dynamic viscosity	$ML^{-1}T^{-1}$
ρ	Water mass density	ML^{-3}

Therefore, the discharge coefficient can be represented as a function of these elements in Eq. (2):

$$Cd = f(V_1, y_1, p, B, L, \ell, \rho, \mu, g, \alpha, \theta) \quad (2)$$

By applying the Buckingham π-theorem, the final dimensionless expression after eliminating the parameters that do not affect the estimation of the discharge coefficient over labyrinth side weirs was derived and is presented in Eq. (3):

$$Cd = f\left(\frac{p}{y_1}, \frac{B}{y_1}, Fr_1, \alpha, \theta\right) \quad (3)$$

Eq. (3) reflects the factors influencing the discharge coefficient of the labyrinth side weir in this study.

4. EXPERIMENTAL WORKS

The experiments were carried out in a main and lateral laboratory flume, as shown in Figure 3. The main flume is 6 m long and 0.5 m wide rectangular main flume with tempered glass sidewalls and an almost horizontal, smooth bed. A 30° inlet baffle was installed to reduce upstream turbulence. To promote flow stability, a 0.50 m side opening was located 4.2 m downstream of the inlet, and water was supplied by a pump system (maximum discharge: 139,800 L/hr) controlled through a manual valve. Before each test, flow stabilization was confirmed for a few minutes. Discharge in both the main and lateral channels is then measured using a sharp-crested V-notch weir, calibrated by repeating discharge measurements three times for twenty different flow conditions; average values were used in the analysis. Two-point gauges with 0.01 mm sensitivity are used to measure the head. The labyrinth side-weir models, designed according to the studies [8, 28] using AutoCAD and CNC-cut from 1.5 mm UV-resistant flexible plastic, featured a crest height of P = 10 cm and were installed on a 50 cm bed projection, with 4 cm free space on each side for adequate nappe aeration (see Figure 4). During each run, water-surface profiles along the main flume were recorded using nine ultrasonic sensors connected to a data collector system, with manual checks for verification. The collected data were displayed on a laptop for analysis, and additional manual checks are outlined in Figure 5. All instruments were carefully calibrated before testing. Throughout the experiments, potential error sources such as pump discharge fluctuations, sensor shift, point-gauge reading

variability, and temperature-related water property changes were controlled by repeated measurements, averaging, and continuous monitoring of flow stability. Regular investigations of the flume ensured uniform conditions and proper alignment of the weirs. These measures collectively reduced experimental uncertainty and improved the discharge coefficient results.

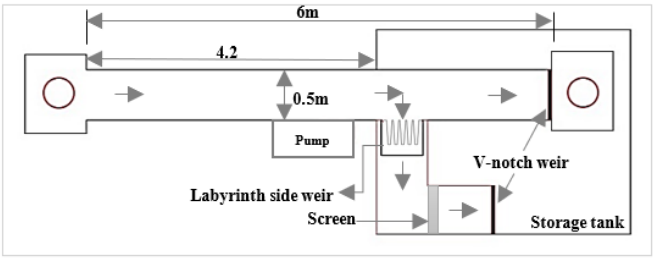

Figure 3. An experimental flume schematic setup

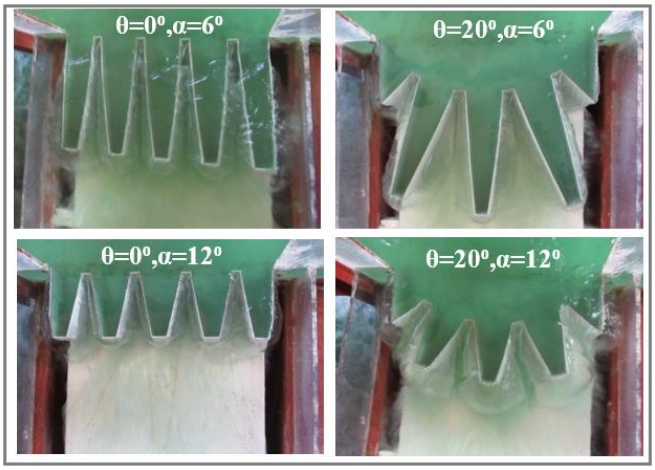

Figure 4. Experimental side weir configurations (5 cycles)

Figure 5. Installation of sensors with a data collector

5. RESULTS AND DISCUSSION

Energy values at the upstream and downstream ends of the side weir were calculated to assess the specific energy variation along the weir, as shown in Figure 6. The minimal average specific energy variation of 0.78% between the two ends of the side weir, derived from Eq. (4), confirms that the specific energy can be considered constant. This finding validates the use of the De-Marchi Eq. (1) for calculating discharge coefficients in all test cases and supports its reliability for design and hydraulic modeling of side weirs. The experimental results summarized in Table 2 provide further evidence for this conclusion.

$$\text{Energy differences } (\Delta E\%) = \frac{100}{N}\sum_{i=1}^{N}(E_2 - E_1) \qquad (4)$$

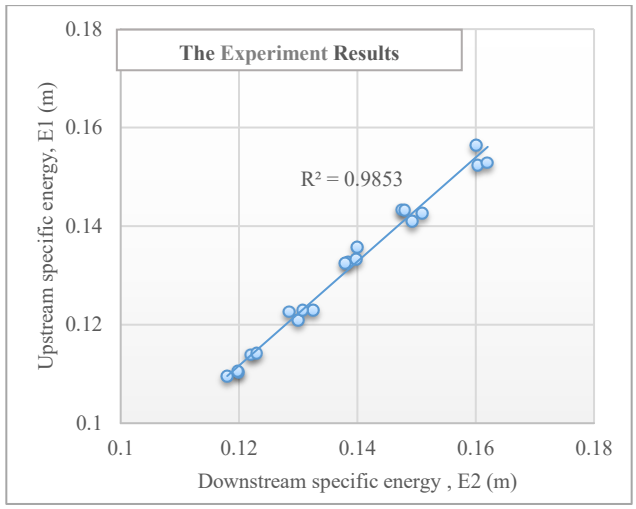

Figure 6. Specific energy difference at the upstream E1 and downstream E2 ends of the side weir for all tests

Table 2. Experimental data for all tests

Side Weir Model	Sidewall Angle (α)	Model Symbol	Fr_1	Cd
Trapezoidal (θ = 0°)	6°	TSW6	0.08-0.25	1.18-3.07
	12°	TSW12	0.08-0.20	0.95-1.84
Arced-Trapezoidal (θ = 20°)	6°	ATSW6	0.10-0.23	1.51-4.04
	12°	ATSW12	0.06-0.20	1.01-2.17

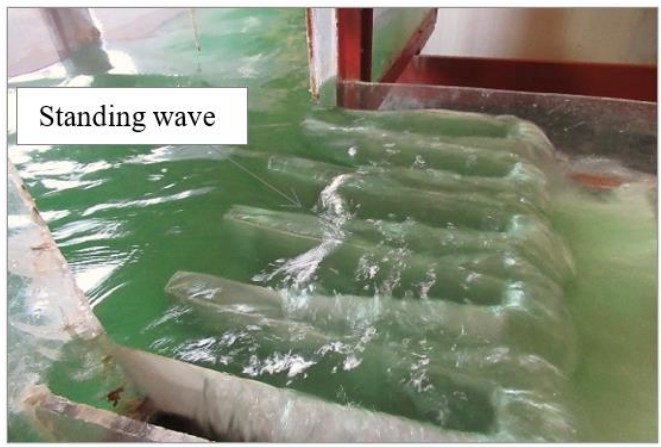

Figure 7. The laboratory notes for the standing wave phenomenon

In all the experimental tests, the flow depth at the upstream end of the side weir was smaller than at the downstream end.

The longitudinal water surface profile shows a slight decrease at the weir entrance and the formation of turbulence because of the impact with the weir wall, as shown in Figure 7. The results aligned with other researchers' studies [5, 7, 29].

The water level decreases from the flume side wall towards the edge of the weir. It then suddenly rises as a standing wave phenomenon is formed due to the weir sill and the interference of the approach flow, which was clear in the visual notes for the trapezoidal labyrinth side weir model in Figure 7. In contrast, the flow was more uniform for the arced-trapezoidal side-weir model. The water outlets create a hydraulic jump due to the increase in the mean velocity; therefore, specific energy dissipation increases [30].

Figure 8 represents the points of measurement of water elevation at the centerline (25 cm) of the main flume and 10 cm from the side bank near the weir for uniform distances. These points were shown in Figures 9-10 to plot the free surface profile along the main flume upstream and downstream of the side weir of this study. The water surface profile of the centerline increased uniformly, and then, after the downstream end of the side weir, it became almost horizontal. In contrast, the water elevation near the flume bank varies along the weir width because of the side weir inlet friction. As the flow depth decreases, maximum velocity at the onset of the weir crest forms a vortex due to the secondary flow because of the change in flow direction.

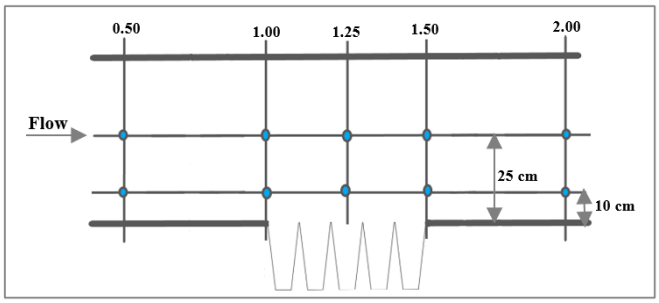

Figure 8. Plan view for the points of measuring

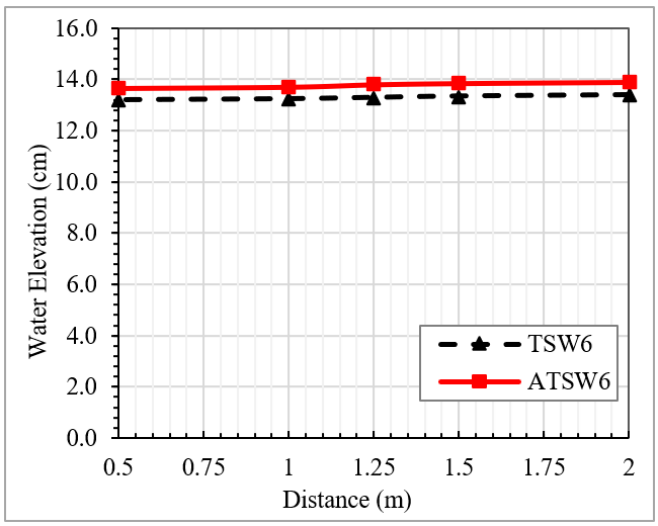

Figure 9. Free surface profile along centerline of main flume for side weir models with sidewall angle 6°, Q_{in} = 17 L/s

In contrast, the depth increases at the weir end, where the minimum velocity forms a stagnation zone due to flow separation. The effect of the weir inlet provided near the weir crest does not reach the midspan main flume, which aligns with previous studies. Due to the steady flow conditions observed in this region, most previous studies have focused on the flow depth at the upstream end of the side weir at the center of the main flume [7, 8, 23, 29, 31]. Therefore, this study has considered the flow depth (y_1), as in the literature. Therefore, the results of this study can be contrasted with those of previous research.

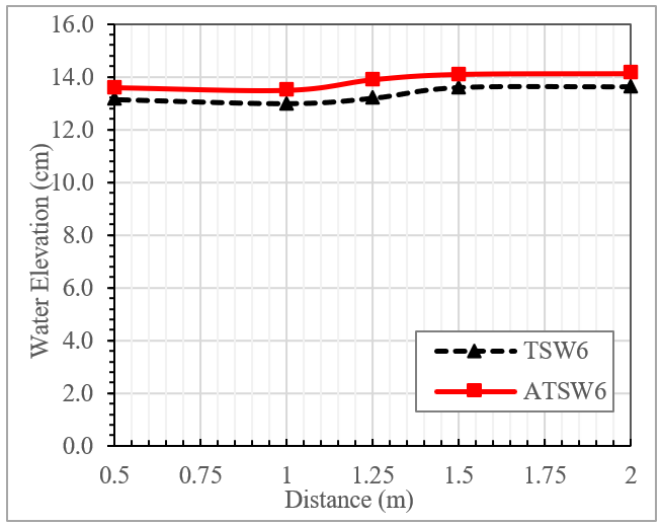

Figure 10. Free surface profile 10 cm from bank, near side weirs models with sidewall angle 6o, Q_{in} = 17 L/s

Figures 11 and 12 illustrate the influence of the relative weir height (p/y_1) on the discharge coefficient (C_d). The results indicate that Cd increases with p/y_1. Models with a sidewall angle of 6° exhibited the highest discharge coefficients (C_d = 1.5–4), primarily due to their longer effective crest length, which enhances flow performance, as reported by the research [32]. Moreover, the arced-trapezoidal labyrinth side weirs (ATSW) produced higher C_d values than the corresponding trapezoidal (TSW) configurations, owing to smoother flow transitions and reduced separation losses along the curved crest.

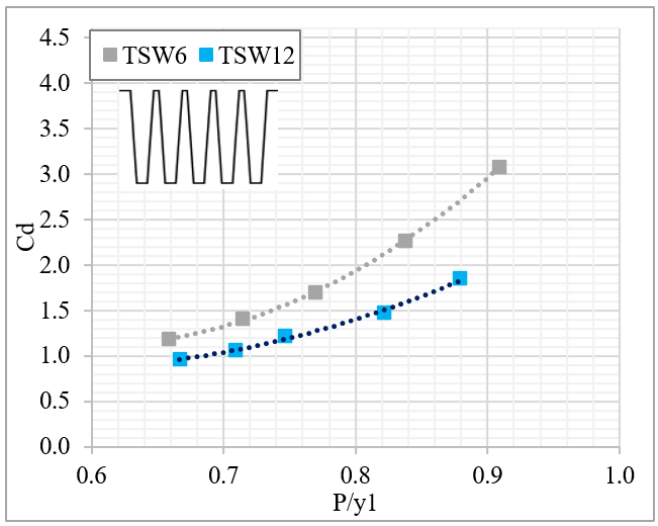

Figure 11. Influence of the parameter p/y1 on the discharge coefficient Cd for trapezoidal labyrinth side weirs (6°, 12°)

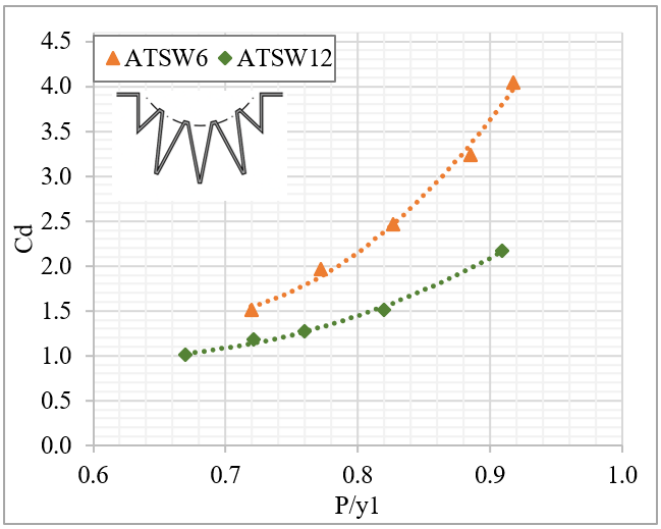

Figure 12. Influence of the parameter p/y1 on the discharge coefficient Cd for arced-trapezoidal labyrinth side weirs (6º, 12º)

The optimum hydraulic performance was observed in the ATSW6 configuration, which combines the benefits of curvature and a smaller sidewall angle. For the same p/y_1 ratios, slight variations in *Cd* were observed. This scatter is mainly attributed to differences in the Froude number (Fr) and other influencing variables included in Eq. (3). These parameters were therefore analyzed to understand their combined effects on *Cd*. Additionally, the same was obtained; the discharge coefficient increased with B/y_1, as shown in Figure 13.

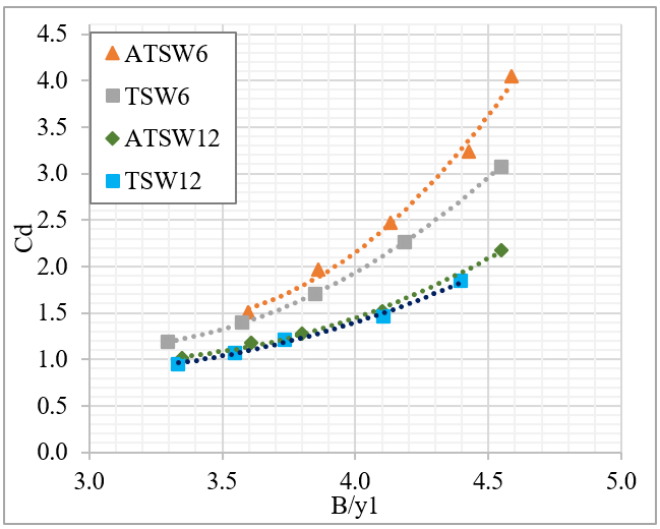

Figure 13. Influence of the parameter B/y1 on the discharge coefficient Cd for different labyrinth side weirs

Studies have consistently shown that the Froude number (*Fr*) is a considerable dimensionless parameter that mainly influences the discharge coefficient (*Cd*) for side weirs, particularly under subcritical flow conditions. Figure 14 plots the calculated discharge coefficient values with the upstream Froude number (Fr_1) for different types of side weirs. This figure shows an inverse relationship between the discharge coefficient and the upstream Froude number across all tests, in agreement with previous studies [13, 33-36].

However, when increasing the entrance discharge, the velocity of flow towards the side weir increases, and the momentum rises; separation and vortices due to secondary flow and surface fluctuations appear, reducing the capacity of side weirs and consequently decreasing the discharge coefficient.

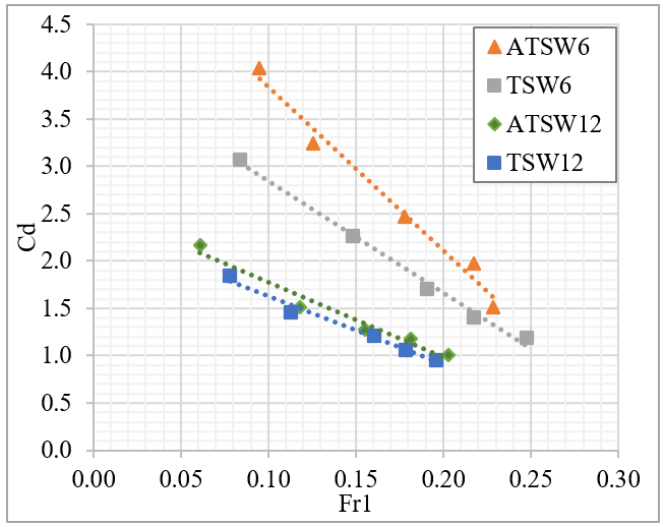

Figure 14. Influence of upstream Froude number Fr_1 on the discharge coefficient Cd for different labyrinth side weirs

Figures 15 and 16 compare the distribution of average flow velocity and pressure, respectively, along the two ends of the side weir for two models: TSW6 and ATSW6, both with a 6° side wall angle. For the TSW6 model, there is a sharp rise in velocity (0.54 m/s) at the onset crest, followed by a gradual decrease (0.29 m/s). In contrast, pressure in the TSW6 model drops at the upstream (0.8 Pa), then it increases to 2 Pa, consistent with Bernoulli's theory, which predicts an inverse relationship between velocity head and pressure head in open channels.

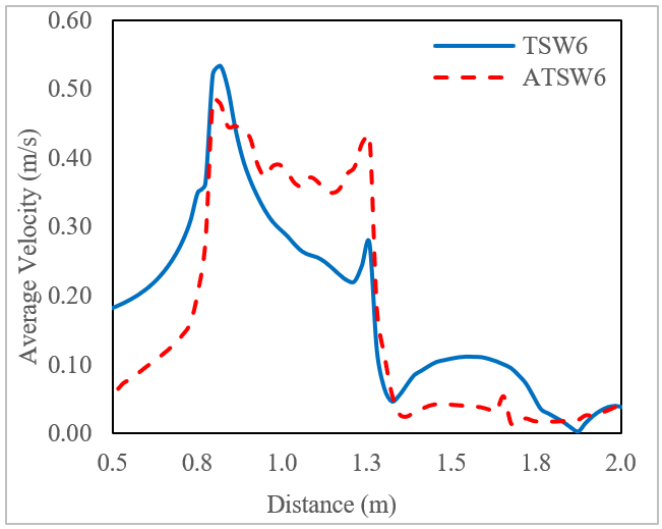

Figure 15. The mean velocity distribution at both ends of different labyrinth side weirs

In contrast, in the ATSW6 model, the pattern shifts: it shows a smoother rise in velocity and a lower peak magnitude between (0.50 and 0.42) m/s. This behavior suggests that the curvature of the arced crest in ATSW6 promotes more gradual

energy conversion, minimizes local flow separation, and ensures a steadier pressure field range (4-45) Pa.

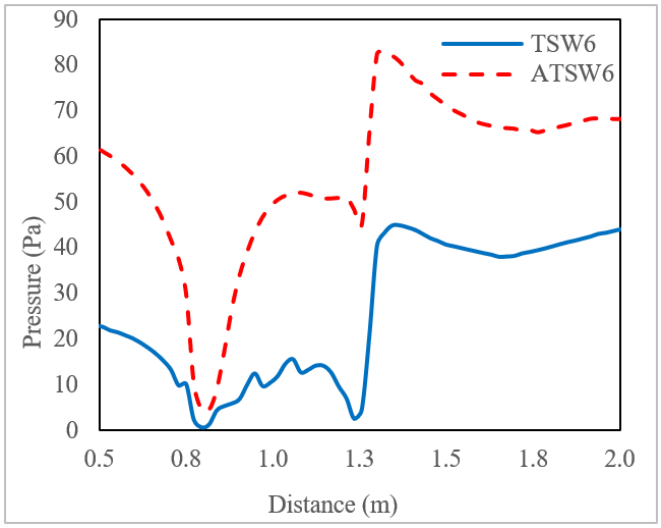

Figure 16. The pressure distribution at both ends of different labyrinth side weirs

6. THE SIDE WEIR EQUATION BY REGRESSION ANALYSIS

In this study, SPSS 22 software was used by nonlinear regression analysis to develop an empirical relationship to predict the discharge coefficient (Cd) for side weirs, according to the effective parameters of dimensional analysis influencing its discharge characteristics, the upstream Froude number (Fr_1), (P/y_1), and (B/y_1) ratios. The resulting discharge coefficient formulas are provided as follows in Eqs. (5)-(8) as presented in Table 3.

Table 3. Discharge coefficient equations for the various labyrinth side weir models

Side Weir Model	Equation	No.
ATSW6	$Cd = 0.329\frac{\left(\frac{p}{y_1}\right)^{1.464}\left(\frac{B}{y_1}\right)^{1.192}}{(Fr_1)^{0.345}}$	(5)
TSW6	$Cd = 0.282\frac{\left(\frac{p}{y_1}\right)^{0.999}\left(\frac{B}{y_1}\right)^{1.245}}{(Fr_1)^{0.241}}$	(6)
ATSW12	$Cd = 0.147\frac{\left(\frac{B}{y_1}\right)^{1.064}}{(Fr_1)^{0.382}\left(\frac{p}{y_1}\right)^{0.126}}$	(7)
TSW12	$Cd = 0.148\frac{\left(\frac{p}{y_1}\right)^{0.113}\left(\frac{B}{y_1}\right)^{1.155}}{(Fr_1)^{0.322}}$	(8)

To ensure the accuracy and precision of the developed equations in the present studies [32, 37], the Root Mean Square Error (RMSE) and average percent errors (APE) values are calculated as Eq. (9) and (10) in addition to the determination coefficient R^2 directly from the SPSS program for the measured discharge coefficient Cd of experimental values against the proposed ones in Eq. (5-8) as presented in Table 4. The results showed the measurement precision of the equations, with maximum RMSE and APE of 2% and 5%, respectively, and an R^2 of about 0.99 for discharge coefficient prediction.

$$RMSE = 100 \times \sqrt{\frac{1}{N}\sum_{i=1}^{N}\left(Cd_{exp.} - Cd_{proposed}\right)^2} \quad (9)$$

$$APE = \frac{100}{N}\sum_{i=1}^{N}\left|\frac{Cd_{exp.} - Cd_{proposed}}{Cd_{exp.}}\right| \quad (10)$$

where, $Cd_{exp.}$ and $Cd_{proposed}$ represent the comparison of the discharge coefficient of experimental results and its proposed values of the empirical equations, where $N$is the total number of data.

Table 4. The statistical parameters for estimating the accuracy of equations

Side Weir Model	Equation No.	R^2	RMSE	APE
ATSW6	(5)	0.997	4.89%	1.93%
TSW6	(6)	0.998	2.89%	1.64%
ATSW12	(7)	0.998	1.70%	1.10%
TSW12	(8)	0.996	2.10%	1.37%

7. CONCLUSIONS

Labyrinth side weirs are nonlinear hydraulic structures that enhance lateral discharge in open channels. Flow over these weirs is influenced by multiple variables, including: (α, θ, p/y_1, B/y_1, and Fr_1). This laboratory study aims to develop an analytical approach to estimate flow on several geometric configurations of labyrinth side weirs in a straight channel, considering the variables that influence it. The following key findings were investigated from these experiments:

- It has been proven that the De-Marchi equation to calculate the discharge coefficient can be used for all the tests of this study.
- Also, the efficiency of labyrinth side weirs for both trapezoidal and arced-trapezoidal geometries increase with a decrease of sidewall angle from (α = 12° to 6°). This is because of the increased length of the path of flow over the folded crest of the side weir, with constant weir width, which increases the average velocity through the greater effect of secondary flow, thereby affecting the discharge coefficient values.
- In addition, comparison of the performance of arced-trapezoidal side weirs with an arc cycle angle (θ = 20°) to trapezoidal models (θ = 0°) shows higher effectiveness in the arced-trapezoidal models due to the curvature, which enhances the discharge coefficient and increases flow stability through improved flow guidance and reducing hydraulic losses.
- Moreover, among the tested models, the optimum side weir was found to be the arced-trapezoidal geometry with a sidewall angle (α = 6°), which exhibited the highest discharge coefficient, with a range of Cd (1.51-4.04), followed by trapezoidal with a sidewall angle (α = 6°), arced-trapezoidal geometry with a sidewall angle (α = 12°), and trapezoidal with sidewall angle (α = 12°), respectively.

- Furthermore, the discharge coefficient (Cd) was observed to gradually increase with both the ratio of weir height to water depth (p/y_1) and the ratio of channel width to water depth (B/y_1), while it gradually decreases as the upstream Froude number (Fr_1) increases in the subcritical flow conditions of this study.
- Finally, nonlinear regression analysis was applied to develop analytical equations for estimating discharge for each model based on dimensional analysis parameters. The four resulting equations exhibited strong agreement with experimental data, with accuracy assessed using RMSE, APE, and R^2, which were 5%, 2%, and 0.99, respectively.

ACKNOWLEDGMENT

The College of Engineering at Tikrit University, Iraq, supported the laboratory work for this study.

REFERENCES

[1] Ansari, U.S., Patil, L.G. (2019). Flow over side weirs with experimental & CFD results. International Journal of Engineering and Advanced Technology, 9(1): 1315-1319. https://doi.org/10.35940/ijeat.A9650.109119

[2] Alfatlawi, T.J., Hashem, T., Hasan, Z.H. (2023). Discharge coefficient of symmetrical stepped and triangular labyrinth side weirs in a subcritical flow regime. Journal of Irrigation and Drainage Engineering, 149(4): 04023004. https://doi.org/10.1061/jidedh.ireng-9627

[3] Hussein, B.S., Jalil, S.A. (2020). Hydraulic performance for combined weir-gate structure. Tikrit Journal of Engineering Sciences, 27(1): 40-50. https://doi.org/10.25130/tjes.27.1.06

[4] Emin Emiroglu, M., Cihan Aydin, M., Kaya, N. (2014). Discharge characteristics of a trapezoidal labyrinth side weir with one and two cycles in subcritical flow. Journal of Irrigation and Drainage Engineering, 140(5): 04014007. https://doi.org/10.1061/(asce)ir.1943-4774.0000709

[5] Tullis, J.P., Amanian, N., Waldron, D. (1995). Design of labyrinth spillways. Journal of Hydraulic Engineering, 121(3): 247-255. https://doi.org/10.1061/(ASCE)0733-9429(1995)121:3(247)

[6] Emin Emiroglu, M., Kaya, N., Agaccioglu, H. (2010). Discharge capacity of labyrinth side weir located on a straight channel. Journal of Irrigation and Drainage Engineering, 136(1): 37-46. https://doi.org/10.1061/(ASCE)IR.1943-4774.0000112

[7] Emiroglu, M.E., Kaya, N. (2011). Discharge coefficient for trapezoidal labyrinth side weir in subcritical flow. Water Resources Management, 25(3): 1037-1058. https://doi.org/10.1007/s11269-010-9740-7

[8] Crookston, B.M., Tullis, B. (2010). Labyrinth weirs. Hydraulic Structures, 59. https://digitalcommons.usu.edu/etd/802.

[9] Monjezi, R., Heidarnejad, M., Masjedi, A., Purmohammadi, M.H., Kamanbedast, A. (2018). Laboratory investigation of the Discharge Coefficient of flow in arced labyrinth weirs with triangular plans. Flow Measurement and Instrumentation, 64: 64-70. https://doi.org/10.1016/j.flowmeasinst.2018.10.011

[10] Borghei, S.M., Nekooie, M.A., Sadeghian, H., Ghazizadeh, M.R.J. (2013). Triangular labyrinth side weirs with one and two cycles. In Proceedings of the Institution of Civil Engineers-Water Management, 166(1): 27-42. https://doi.org/10.1680/wama.11.00032

[11] Karimi, M., Ghazizadeh, M.J., Saneie, M., Attari, J. (2019). Flow characteristics over asymmetric triangular labyrinth side weirs. Flow Measurement and Instrumentation, 68: 101574. https://doi.org/10.1016/j.flowmeasinst.2019.101574

[12] Dogan, Y., Kaya, N. (2023). The effects of changing the effective crest length of labyrinth side weir on discharge capacity. Arabian Journal for Science and Engineering, 48(4): 5289-5304. https://doi.org/10.1007/s13369-022-07388-y

[13] Aydin, M.C., Emin Emiroglu, M. (2016). Numerical analysis of subcritical flow over two-cycle trapezoidal labyrinth side weir. Flow Measurement and Instrumentation, 48: 20-28. https://doi.org/10.1016/j.flowmeasinst.2016.01.007

[14] Rustiati, N.B., Ishak, M.G., Tanga, A., Pali, Z.G. (2023). Influence of the number of trapezoidal labyrinth weir cycles on the hydraulic characteristics of the weir. IOP Conference Series: Earth and Environmental Science, 1157(1): 012051. https://doi.org/10.1088/1755-1315/1157/1/012051

[15] Ahmad, F., Hussain, A., Ansari, M.A. (2023). Development of ANN model for the prediction of discharge coefficient of an arced labyrinth side weir. Modeling Earth Systems and Environment, 9(2): 1835-1842. https://doi.org/10.1007/s40808-022-01593-2

[16] Feili, J., Heidarnejad, M., Kamanbedast, A.A., Masjedi, A., Asadi Lor, M. (2020). Experimental study of discharge coefficient of trapezoidal arced labyrinth weirs with different arc radius and cycle length. Iranian Journal of Soil and Water Research, 51(5): 1115-1126. https://doi.org/10.22059/ijswr.2020.293163.668411

[17] Thompson, E.A., Cox, N.C., Ebner, L.L., Tullis, B.P. (2016). The hydraulic design of an arced labyrinth weir at Isabella Dam. In 6th International Symposium on Hydraulic Structures: Hydraulic Structures and Water System Management, Portland, OR, pp. 148-157. https://doi.org/10.15142/T3280628160853

[18] Christensen, N.A., Tullis, B.P. (2012). Arced Labyrinth Weir Flow Characteristics. https://digitalcommons.usu.edu/ewhs/Sessions/1/1.

[19] Khalili, M., Honar, T. (2017). Discharge coefficient of semi-circular labyrinth side weir in subcritical flow. Water SA, 43(3): 433-441. https://doi.org/10.4314/wsa.v43i3.08

[20] Sangsefidi, Y., Mehraein, M., Ghodsian, M., Motalebizadeh, M.R. (2017). Evaluation and analysis of flow over arced weirs using traditional and response surface methodologies. Journal of Hydraulic Engineering, 143(11): 04017048. https://doi.org/10.1061/(asce)hy.1943-7900.0001377

[21] Alfatlawi, T.J., Alkafaji, R.D.M. (2023). Effect of anti-vortex structures installed on stepped labyrinth side weirs on discharge capacity. Flow Measurement and Instrumentation, 89: 102307. https://doi.org/10.1016/j.flowmeasinst.2023.102307

[22] Subramanya, K., Awasthy, S.C. (1972). Spatially varied flow over side-weirs. Journal of the Hydraulics Division, 98(1): 1-10. https://doi.org/10.1061/JYCEAJ.0003188
[23] Borghei, S.M., Jalili, M.R., Ghodsian, M. (1999). Discharge coefficient for sharp-crested side weir in subcritical flow. Journal of Hydraulic Engineering, 125(10): 1051-1056. https://doi.org/10.1061/(ASCE)0733-9429(1999)125:10(1051)
[24] Marchi, D. (1934). Essay on the performance of lateral weirs. L'Energia Elettrica, Milan, Italy, 11: 849-860.
[25] Ramamurthy, A.S., Qu, J., Vo, D. (2006). Nonlinear PLS method for side weir flows. Journal of Irrigation and Drainage Engineering, 132(5): 486-489. https://doi.org/10.1061/(ASCE)0733-9437(2006)132:5(486)
[26] Chow, V.T. (1959). Open Channel Hydraulics. MacGraw-Hill Book Co. Inc., New York, NY, 206. https://www.scribd.com/document/684578636/19-Ven-Te-Chow-Open-Channel-Hydraulics-Mcgraw-Hill-College-1959.
[27] Szirtes, T., Rózsa, P. (2007). Applied Dimensional Analysis and Modeling. Butterworth-Heinemann. https://doi.org/10.1016/B978-0-12-370620-1.X5000-X
[28] Crookston, B.M., Tullis, B.P. (2012). Arced labyrinth weirs. Journal of Hydraulic Engineering, 138(6): 555-562. https://doi.org/10.1061/(ASCE)HY.1943-7900.0000553.
[29] Agaccioglu, H., Yüksel, Y. (1998). Side-weir flow in curved channels. Journal of irrigation and drainage engineering, 124(3): 163-175. https://doi.org/10.1061/(ASCE)0733-9437(1998)124:3(163)
[30] Jamel, A.A.J., Tawfeeq, S.S., Abed Hussain, R. (2025). Improving energy dissipation on stepped spillways (numerical simulation). International Review of Civil Engineering (IRECE), 16(3): 201-210. https://doi.org/10.15866/irece.v16i3.25616
[31] Hager, W.H. (1987). Lateral outflow over side weirs. Journal of Hydraulic Engineering, 113(4): 491-504. https://doi.org/10.1061/(ASCE)0733-9429(1987)113:4(491)
[32] Hussain, R.A., Hassan, S.A., Jamel, A.A.J. (2022). Experimental study on flow over triangular labyrinth weirs. International Journal of Design & Nature and Ecodynamics, 17(2): 249-255. https://doi.org/10.18280/ijdne.170211
[33] Khameneh, H.Z., Khodashenas, S.R., Esmaili, K. (2014). The effect of increasing the number of cycles on the performance of labyrinth side weir. Flow Measurement and Instrumentation, 39: 35-45. https://doi.org/10.1016/j.flowmeasinst.2014.05.002
[34] Hussein, B.S., Jalil, S.A. (2025). Influence of labyrinth side weir shape modification on the hydrodynamic performance: Experimental and numerical study. Arabian Journal for Science and Engineering, 50(16): 12881-12902. https://doi.org/10.1007/s13369-024-09563-9
[35] Izadinia, E., Heidarpour, M. (2016). Discharge coefficient of a circular-crested side weir in rectangular channels. Journal of Irrigation and Drainage Engineering, 142(6): 06016005. https://doi.org/10.1061/(ASCE)IR.1943-4774.0001025
[36] Abbasi, S., Fatemi, S., Ghaderi, A., Di Francesco, S. (2020). The effect of geometric parameters of the antivortex on a triangular labyrinth side weir. Water, 13(1): 14. https://doi.org/10.3390/w13010014
[37] Flayyih, S.S., Jasim, F.H., Nafe'e, O.T., Jamel, A.A.J. (2025). An artificial intelligence-driven evaluation of scour depth around bridge piers. Engineering, Technology & Applied Science Research, 15(5): 26310-26316. https://doi.org/10.48084/etasr.12240